2023

Experimental study on the mechanical controlling factors of fracture plugging strength for lost circulation control in shale gas reservoir

Chengyuan Xu

Lingmao Zhu

Feng Xu

Yili Kang

Haoran Jing

See next page for additional authors

10.1016/j.geoen.2023.212285

Xu, C., Zhu, L., Xu, F., Kang, Y., Jing, H., & You, Z. (2023). Experimental study on the mechanical controlling factors of fracture plugging strength for lost circulation control in shale gas reservoir. Geoenergy Science and Engineering, 231(Part A), article 212285. https://doi.org/10.1016/j.geoen.2023.212285

231 (2023) 212285

Contents lists available at ScienceDirect

Geoenergy Science and Engineering

journal homepage: www.sciencedirect.com/journal/geoenergy-science-and-engineering

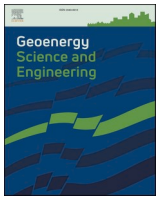

Experimental study on the mechanical controlling factors of fracture plugging strength for lost circulation control in shale gas reservoir

Chengyuan Xu [a,b,**], Lingmao Zhu [a,c], Feng Xu [a], Yili Kang [a], Haoran Jing [a], Zhenjiang You [d,e,f,*]

[a] State Key Laboratory of Oil & Gas Reservoir Geology and Exploitation, Southwest Petroleum University, Chengdu, China
[b] School of Petroleum Engineering, China University of Petroleum (East China), Qingdao, China
[c] PetroChina Changqing Oilfield Company, China
[d] Center for Sustainable Energy and Resources, Edith Cowan University, Joondalup, WA, 6027, Australia
[e] School of Chemical Engineering, The University of Queensland, Brisbane, QLD, 4072, Australia
[f] Centre for Natural Gas, The University of Queensland, Brisbane, QLD, 4072, Australia

ARTICLE INFO

Keywords:
Shale reservoir
Fracture plugging zone strength
Fracture surface
Mechanical properties
Friction coefficient

ABSTRACT

The geological conditions of shale reservoir present several unique challenges. These include the extensive development of multi-scale fractures, frequent losses during horizontal drilling, low success rates in plugging, and a tendency for the fracture plugging zone to experience repeated failures. Extensive analysis suggests that the weakening of the mechanical properties of shale fracture surfaces is the primary factor responsible for reducing the bearing capacity of the fracture plugging zone. To assess the influence of oil-based environments on the degradation of mechanical properties in shale fracture surfaces, rigorous mechanical property tests were conducted on shale samples subsequent to their exposure to various substances, including white oil, lye, and the filtrate of oil-based drilling fluid. The experimental results demonstrate that the average values of the elastic modulus and indwelling hardness of dry shale are 24.30 GPa and 0.64 GPa, respectively. Upon immersion in white oil, these values decrease to 22.42 GPa and 0.63 GPa, respectively. Additionally, the depth loss rates of dry shale and white oil-soaked shale are determined to be 57.12% and 61.96%, respectively, indicating an increased degree of fracturing on the shale surface. White oil, lye, and the filtrate of oil-based drilling fluid have demonstrated their capacity to reduce the friction coefficient of the shale surface. The average friction coefficients measured for white oil, lye, and oil-based drilling fluid are 0.80, 0.72, and 0.76, respectively, reflecting their individual weakening effects. Furthermore, it should be noted that the contact mode between the plugging materials and the fracture surface can also lead to a reduction in the friction coefficient between them. To enhance the bearing capacity of the plugging zone, a series of plugging experiments were conducted utilizing high-strength materials, high-friction materials, and nanomaterials. The selection of these materials was based on the understanding of the weakened mechanical properties of the fracture surface. The experimental results demonstrate that the reduced mechanical properties of the fracture surface can diminish the pressure-bearing capacity of the plugging zone. However, the implementation of high-strength materials, high-friction materials, and nanomaterials effectively enhances the pressure-bearing capacity of the plugging zone. The research findings offer valuable insights and guidance towards improving the sealing pressure capacity of shale fractures and effectively increasing the success rate of leakage control measures during shale drilling and completion.

1. Introduction

As the global energy consumption continues, conventional natural gas resources have been unable to meet the increasing energy demand. With the maturation of hydraulic fracturing and horizontal wells, shale gas has become an important component of natural gas production and energy source. However, losses occur frequently during shale drilling (Fig. 1), leading to the increase of well construction cycle and operational costs. Lost working fluids can also affect wellbore stability and cause formation damage. Loss refers to the flowback from the well less

* Corresponding author. Center for Sustainable Energy and Resources, Edith Cowan University, Joondalup, WA, 6027, Australia
** Corresponding author. State Key Laboratory of Oil & Gas Reservoir Geology and Exploitation, Southwest Petroleum University, Chengdu, China.
E-mail addresses: chance_xcy@163.com (C. Xu), zhenjiang.you@gmail.com (Z. You).

https://doi.org/10.1016/j.geoen.2023.212285
Received 29 January 2023; Received in revised form 8 July 2023; Accepted 26 August 2023
Available online 4 September 2023

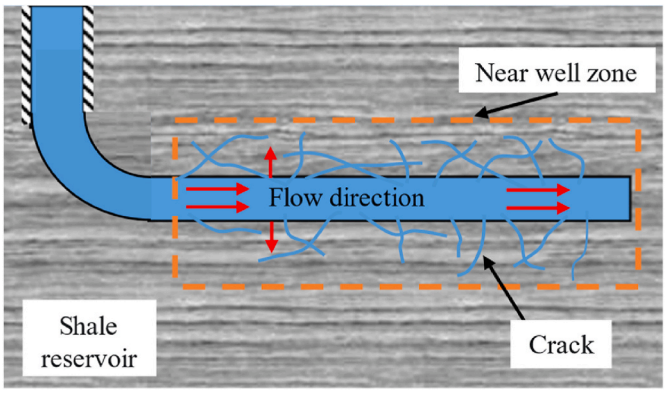

Fig. 1. Schematic diagram of leakage in horizontal Wells.

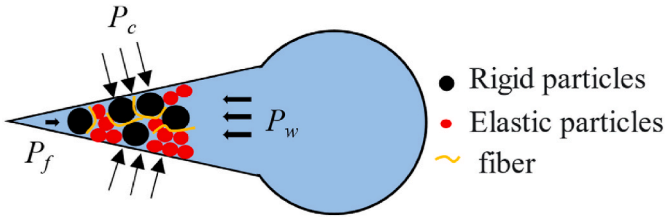

Fig. 2. Particle plugging layer.

than the pumped fluid, which is usually caused by the flow of part or all the well fluid into the formation under the effect of positive pressure gradient (Rehm et al., 2008; Lavrov, 2016; Xu et al., 2019; She et al., 2020). A large number of multi-scale fractures exist in shale reservoirs, and the bearing capacity of borehole walls varies from place to place. The tracking software shows that natural fractures and regional faults exist in the Sichuan-Chongqing shale gas well area. The larger the fault displacement, the more serious the loss. In some blocks, the Longmaxi Formation fractures and micro-fractures have developed, the flexural folds are concentrated, and loss and collapse co-exist (Zheng et al., 2021). The loss of drilling fluid triggers the wellbore stability problem of the horizontal section in shale reservoir which becomes a key factor restricting the efficient development of shale gas (Wang et al., 2008). Enhancing the fracture plugging strength of the shale fracture plugging zone not only effectively controls losses and protects the reservoir, but also enables safe and efficient horizontal drilling.

To prevent overflow, the bottom hole pressure is typically maintained higher than the formation pressure, causing fluid to enter the pore space under pressure. In a porous medium, such as shale, the pressure variations give rise to three distinct zones: the saturated zone, capillary zone, and unsaturated zone. Mohammad et al. simulated fluid flow in a porous medium, validating the applicability of pressure changes in such scenarios (Mohammadizadeh et al., 2021). Notably, an increase in pore pressure within the saturated region can promote the formation and development of microfractures, leading to wellbore instability, drilling fluid loss, and the instability of the plugging zone.

At present, oil-based plugging is the main technology in shale drilling. Physical materials (Fig. 2) are usually used to seal fractures, control drilling fluid loss and wellbore pressure transfer to the fracture tip (Sun et al., 2020). The shale fracture plugging zone is composed of a large number of particles accumulated to form a complex multi-particle system, which is a unified sealing system with the fracture surface and shale rock mass (She, 2016). The fracture plugging strength of the plugging zone determines the quality of the working fluid loss control. Enhancing the bearing capacity of the plugging layer has remained a crucial area of scientific research, with numerous researchers making significant achievements in the study of fracture plugging layer structures. Xu believed that factors affecting the sealing bearing capacity of fractured reservoir included structural failure of the fractured plugging zone, reservoir fracture extension and seepage effect, and analyzed the influence of geometric and mechanical parameters of plugging materials on the sealing bearing capacity of the fractured reservoir (Xu, 2015). Based on the fracture mechanics model, Wang et al. proposed the calculation method of stress intensity factor (SIF) induced at the fracture tip, and analyzed the distribution of pressure in the fracture and the influencing factors of fracture extension after plugging (Wang et al., 2011; Song et al., 2015). Kang et al. summarized the three formation strengthening theories of stress cage, impermeable zone and strong solidification, and established the strengthening model of plugging zone bearing capacity under different guiding theories (Kang et al., 2014a). Yan et al. studied the shear instability strength of fracture plugging zone structure from the perspective of particle material mechanics, and proposed the photo-elastic experimental method to characterize the microstructure of fracture plugging zone (Yan et al., 2020a). Xu et al. pointed out that plugging materials contact with each other to form a force chain network, and the performance parameters of plugging materials determine the strength of the force chain structure (Xu et al., 2020). They proposed that the strength of granular force chain at mesoscale determines the stability of the plugging layer. Based on the mathematical model of sealing strength and the numerical simulation method of

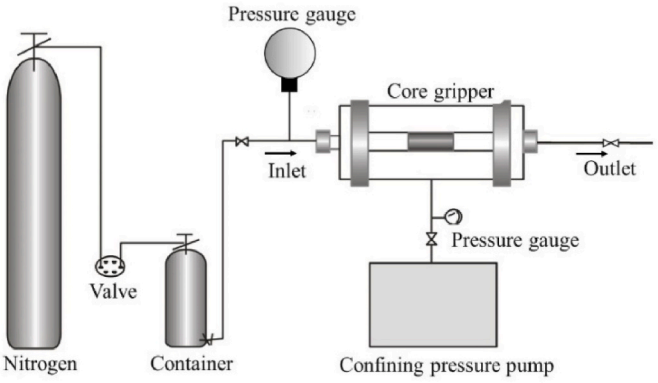

Fig. 4. Flow chart of shale surface weakening device.

Fig. 3. Plugging materials used in the experiment (calcium carbonate, NT-DS, GT-MF, LCC-200 in sequence).

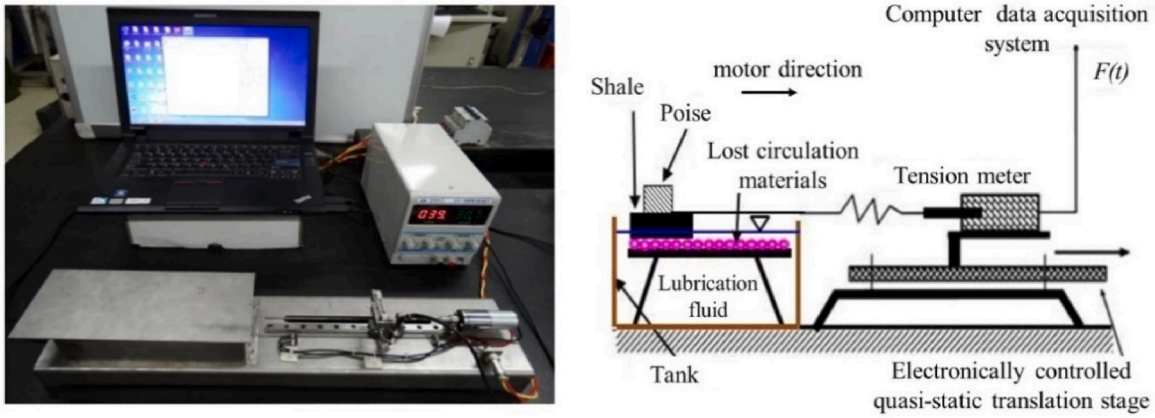

Fig. 5. Schematic diagram of COF-1 friction coefficient measuring system.

Table 1
Plugging material parameters.

Plugging material	Type	Density (g/cm^3)	Diameter (mm)
Calcium carbonate	particle	2.7	1.18 ~ 1.40 mm
NT-DS	powder	1.4–1.6	–
GT-MF	fiber	2.0–2.5	–
LCC 200	fiber	1.02	–

Table 2
Experimental details.

Sample	Experiment fluid	Calculated parameters
A1	–	Elastic modulus E
A2		Indentation hardness H
B1	White oil	
B2		
C1	White oil +1% nanomaterials	
C2		

Table 3
Friction coefficient test experiment.

Sample	Sample quality (g)	Experiment fluid	Immersion time (d)
D1	16.94	White oil	1
D2	16.65		3
D3	14.94		5
D4	16.65		7
D5	12.46		9
D6	13.73		11
D7	27.5		13
E1	24.62	NaOH solution	1
E2	28.33		3
E3	11.65		5
E4	13.23		7
E5	12.61		9
E6	28.55		11
E7	27.22		13
F1	13.23	White oil based drilling fluid filtrate	1
F2	14.12		3
F3	15.11		5
F4	15.64		7
F5	16.19		9
F6	26.11		11
F7	27.27		13
G	33.83	–	–

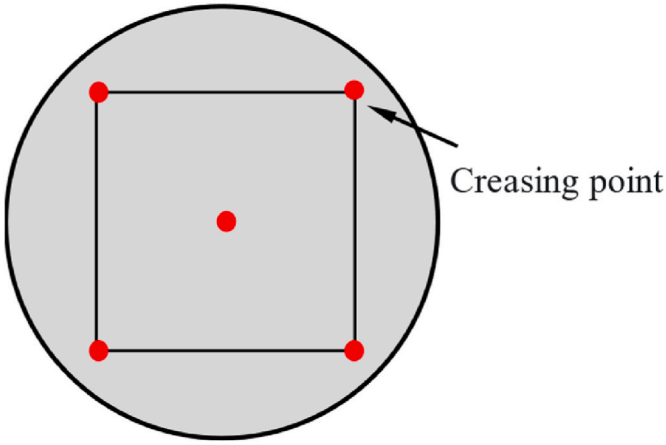

Fig. 6. Micrometer indentation test point.

sealing efficiency, Xu et al. proposed that the friction coefficient of plugging material, a key mechanical parameter, would affect the plugging zone strength and sealing efficiency (Xu et al., 2019). Yan et al. believed that the strong connection network fracture was the micromechanical mechanism of the pressure instability of the fracture plugging zone. They proposed three indexes, the average shear strength of the strong force chains, the development degree of the strong force chains and the geometric structure of the force chain network, as the main controlling factors of the pressure stability of the plugging zone. They developed an evaluation method for the effect of the plugging formula (Yan et al., 2021). Kang et al. found that after high temperature treatment of the plugging material, the pressure bearing capacity of the plugging layer decreased by nearly 50% (Kang et al., 2019). Wang et al. proved that fibers have good temporary plugging effect on natural fractures and induced fractures during fracturing (Wang et al., 2015). Yan et al. reported that the shape and particle size distribution of the LCM, surface friction co-efficient, compressive capacity, abrasion resistance, and temperature resistance are key microscale structure parameters of the fracture plugging zone (Yan et al., 2020b). Xu et al. analyzed the evolution process of the plugging zone and proposed the critical and absolute particle bridging additions by CFD-DEM coupling simulation and photo-elastic experiment (Xu et al., 2021).

While previous studies have predominantly focused on plugging zone models, fluid simulation, and visualization experiments, they have often overlooked the crucial impact of fracture surface mechanical properties on plugging zone pressure. Due to the lye erosion and lubrication effects of the oil-based drilling fluid filtrate on the fracture surface, the mechanism of the influence of weakening mechanical

Table 4
Statistical table of micrometer indentation test data.

Experimental group	E (GPa)				H (GPa)			
	maximum	minimum	average	SD	maximum	minimum	average	SD
A	31.39	19.05	24.30	3.47	0.99	0.39	0.64	0.16
B	27.03	13.19	22.42	3.42	0.91	0.22	0.63	0.17
C	30.76	18.25	23.92	3.48	0.88	0.46	0.62	0.16

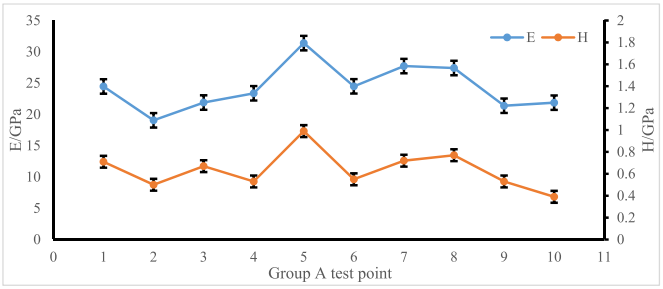

Fig. 7. Group A micron indentation test results.

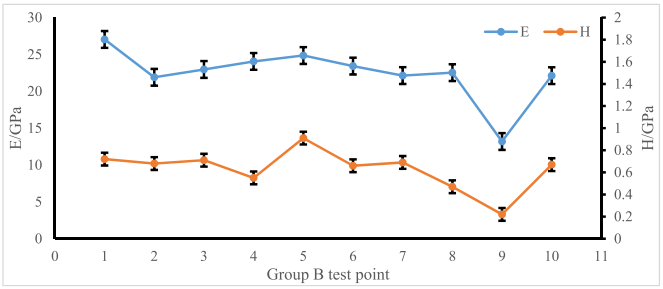

Fig. 8. Group B micron indentation test results.

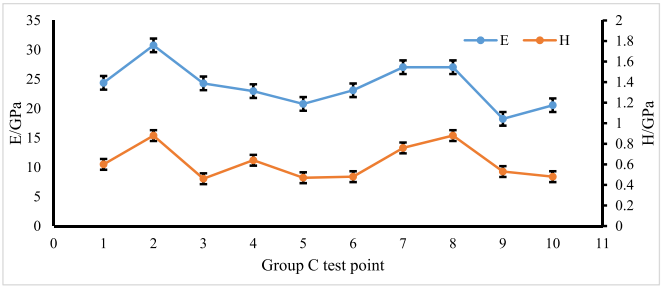

Fig. 9. Group C micron indentation test results.

properties of fracture surface on the pressure of the plugging zone remains unclear. In the second section, we conduct experiments on the weakening of the shale fracture surface subsequent to contact with oil-based drilling fluid. To explore this phenomenon, we employ micron indentation tests and friction coefficient tests. In the third section, we present the experimental data obtained from the previous section, shedding light on the effects observed on the shale surface. In the fourth section, we analyze the mechanism behind the weakening of shale surface mechanical properties and elucidate how these properties influence the pressure within the plugging zone under the presence of oil-based drilling fluids. Furthermore, we perform experiments aimed at strengthening the pressure bearing capacity of the plugging zone based on the weakened fracture surface properties.

2. Factor analysis experiment of pressure bearing capacity of sealing layer

2.1. Rock samples and experimental materials

2.1.1. Sample preparation

The rock samples were selected from the outcrop shale of LMX Formation in the southeast of Chongqing, Sichuan Basin. All the rock samples used in the experiment were processed into small core columns with a diameter of 25 mm and a thickness of about 10 mm by core grinding machine. The core face was sanded with fine sandpaper and was gently blown with nitrogen to obtain a clean, smooth and even end face. After the sample was prepared, it was put into a constant temperature box and continuously dried at 60 °C for 48 h before use.

2.1.2. Experimental materials

The experimental fluid consisted of white oil, NaOH solution (pH = 10), white oil-based drilling fluid filtrate and white oil containing 1% nanomaterials. The materials used in the joint surface friction experiment included calcium carbonate, NT-DS, GT-MF and LCC-200 (see Table 1), which are common bridge filling materials. They were adhered to the friction plate after full mixing to measure the friction coefficient of the joint surface (Fig. 3).

2.2. Experimental method

The purpose of this experiment is to explore the dynamics of shale fracture surface properties after contact with oil-based drilling fluid, analyze the weakening mechanism of shale fracture surface, and discuss the influence of fracture surface weakening on the bearing capacity of plugging zone. The experiment consists of two tests: micron indentation test and friction coefficient test. The details of these tests are provided as follows:

1) Micrometer indentation test of fracture surface

Six spare rock samples were selected and divided into three groups, A, B and C, and numbered. The rock samples were placed in the core gripper and fixed with 5 MPa confining pressure. Nitrogen was used to displace the experimental fluid in contact with the test end face, and the samples were removed 24 h later for micron indentation test. Many scholars have applied micro/nano indentation method to test the micromechanical properties of shale. In this method, small-scale loads are applied to the shale surface through small-size indenter, and mechanical parameters such as elastic modulus, hardness and fracture toughness of shale surface are calculated according to load-displacement curve (Liu et al., 2018a, 2018b; Chen et al., 2015; Shi et al., 2019; Jia et al., 2021; Deirieh et al., 2012; Kumar et al., 2012; Bennett et al., 2015; Alstadt et al., 2015; Zhu et al., 2007).

2) Friction coefficient test of fracture surface

Twenty-one spare rock samples were selected and divided into three groups, D, E and F, and numbered. The rock samples were put into three large beakers, white oil, NaOH solution (pH = 10) and oil-based drilling fluid filtrate were added into the beakers. The rock samples soaked for 1, 3, 5, 7, 9, 11 and 13 days were taken out and the friction coefficient on

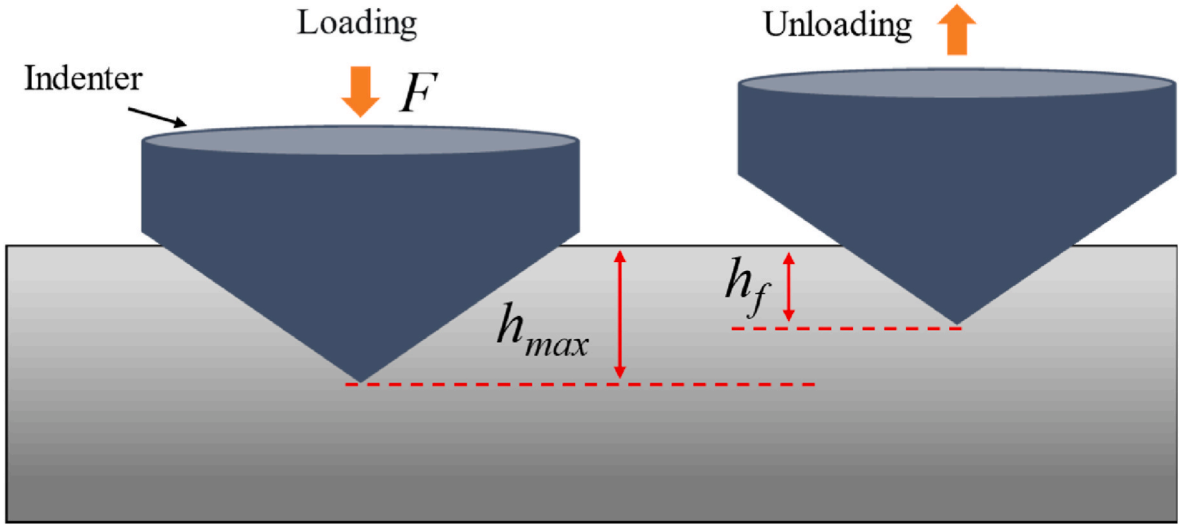

Fig. 10. Schematic of micrometer indentation test.

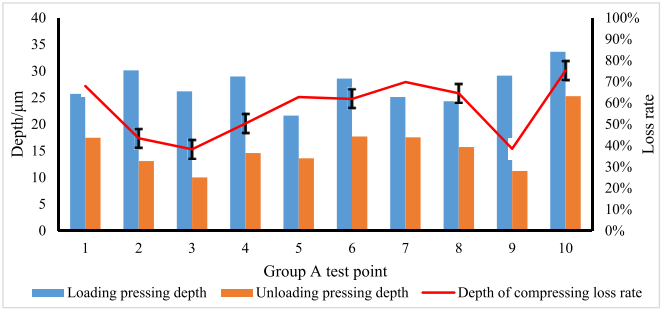

Fig. 11. Pressing depth of Group A shale surface.

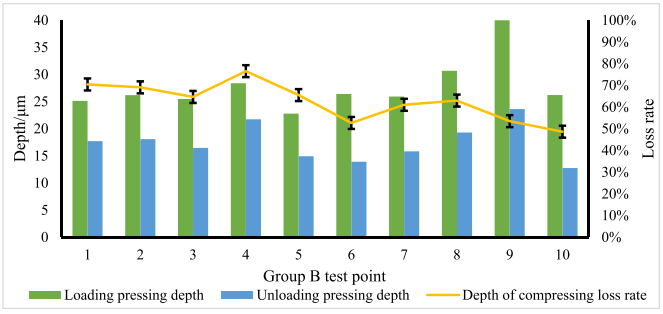

Fig. 12. Pressing depth of Group B shale surface.

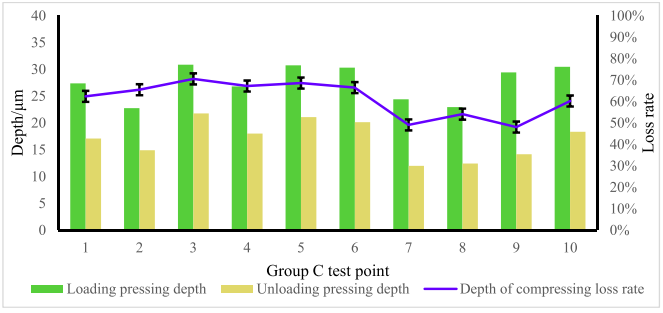

Fig. 13. Pressing depth of Group C shale surface.

Table 5
Friction coefficient of 3 groups of rock samples.

Sample	Friction coefficient	
	First	Second
G	1.04	–
D1	0.88	0.90
D2	0.80	0.71
D3	0.85	0.72
D4	0.78	0.74
D5	0.83	0.65
D6	0.71	0.72
D7	0.73	1.00
E1	0.68	0.68
E2	0.63	0.56
E3	0.75	0.60
E4	0.71	0.60
E5	0.39	0.44
E6	0.73	0.82
E7	0.78	0.76
F1	0.77	0.78
F2	0.80	0.73
F3	0.67	0.71
F4	0.82	0.89
F5	0.77	0.60
F6	0.73	0.60
F7	0.73	0.77

the surface of the rock samples was measured with COF-1 friction coefficient measuring instrument. The friction coefficient can be calculated by the formula (Kang et al., 2019):

$$\mu_f = \frac{F_f}{9.8 \times W_N} \tag{2-1}$$

where μ_f is the friction coefficient, dimensionless; F_f is the tension value recorded by the sensor, namely friction force, N; W_N is the mass of friction slider, kg.

2.2.1. Experimental device

As shown in Fig. 4, this instrument is used to weaken the mechanical properties of the shale surface. The process involves placing the shale into the core gripper, allowing the fluid to contact the shale surface under pressure, and subsequently conducting micron indentation tests after removing the shale. For this study, we employed the UNHT nanoindentation instrument manufactured by Anton Paar. The instrument has a maximum load capacity of 10N, a load accuracy of 0.1 mN, a

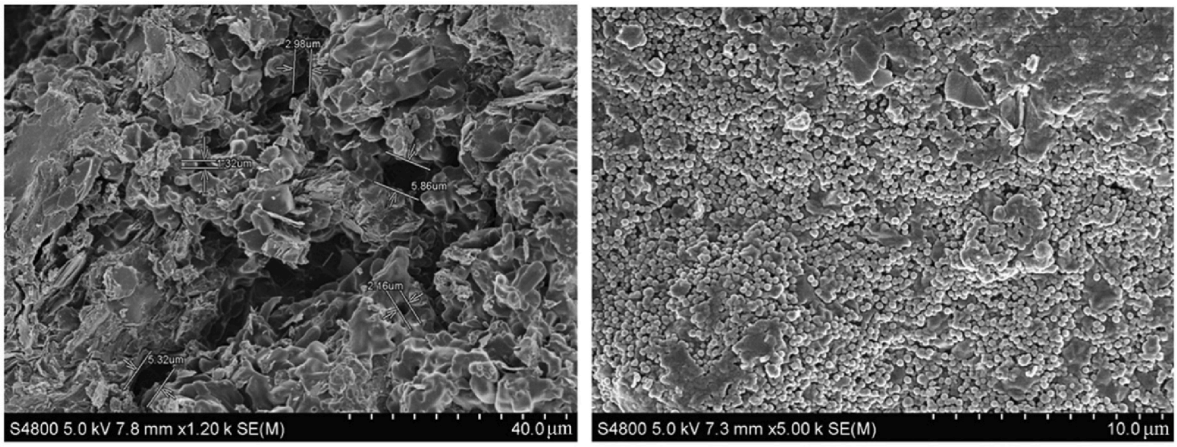

Fig. 14. SEM of shale end face (Wang, 2020) (a) before the nanoparticles plugging the shale; (b) after the nanoparticles plugging the shale.

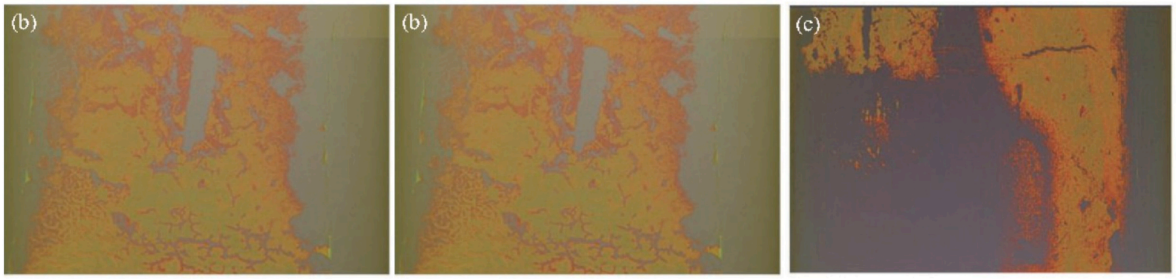

Fig. 15. CT images of shale before and after nanoparticles plugging (Ni et al., 2021), Fluid without nanoparticles: (a) before processing; (b) after processing, Fluids containing nanoparticles: (c) after processing.

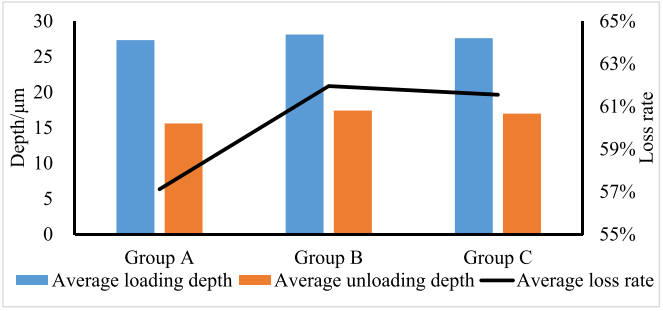

Fig. 16. Pressing depth and loss rate of rock samples in three Group.

loading/unloading rate of 10N/min, an indenter pressure speed of 30000 nm/min, an indenter return speed of 16600 nm/min, and a stability time of 10s at the maximum load.

Fig. 5 shows the COF-1 friction coefficient measuring instrument. The device is primarily composed of a test system and a data acquisition system. During the test, the shale is subjected to a pulling force, causing it to move to the right and come into contact with LCMs. The data acquisition system records the pulling motion in real time, capturing the friction coefficient measurements. The main technical indicators include: ① working temperature: normal temperature ~100 °C; ② friction block mass: 10~100g; (3) maximum travel of linear slide guide: 150 mm; ④ voltage and speed of synchronous motor: DC6~30V, 100R/min; ⑤ lead screw torque: 1.5 kg/cm; ⑥ sliding friction block forward speed: 0–20 cm/min continuous adjustable; ⑦ data acquisition: synchronous acquisition of tension, displacement, time; ⑧ constant temperature liquid tank: rectangular, 200 mm long, 100 mm wide, 20 mm deep; ⑨ tension sensor: range: 0–200g, sensitivity: 0.8 ± 0.1, comprehensive error: 0.05%FS.

2.2.2. *Experimental procedure*

(1) **Micrometer indentation test of crack surface**

(1) Six spare rock samples were divided into A, B and C groups and numbered as A1, A2, B1, B2, C1 and C2.
(2) Put A1 rock sample into the core gripper. When the test end face is toward the inlet direction, apply 5 MPa confining pressure to the confining pressure pump, connect the pipeline and check the air tightness of the device.
(3) Add 500 mL white oil to the intermediate container and connect the pipelines.
(4) Pressurize the nitrogen cylinder slowly. Observe the pressure gauge at the entrance of the gripper. Stop pressurizing when the inlet pressure reaches 1.5 MPa. Keep the pressure of 1.5 MPa for 24 h, take out the rock sample, carefully absorb the residual white oil on the end face with oil-absorbing paper, and let it dry. The micron indentation test was performed on A1 (as shown in Fig. 6), and the elastic modulus and inputting hardness of the end face of A1 were obtained by processing the load-displacement curve with Oliver-Pharr method.
(5) The elastic modulus and compression hardness of A2, B1, B2, C1 and C2 were calculated by the same method. Group B rock sample

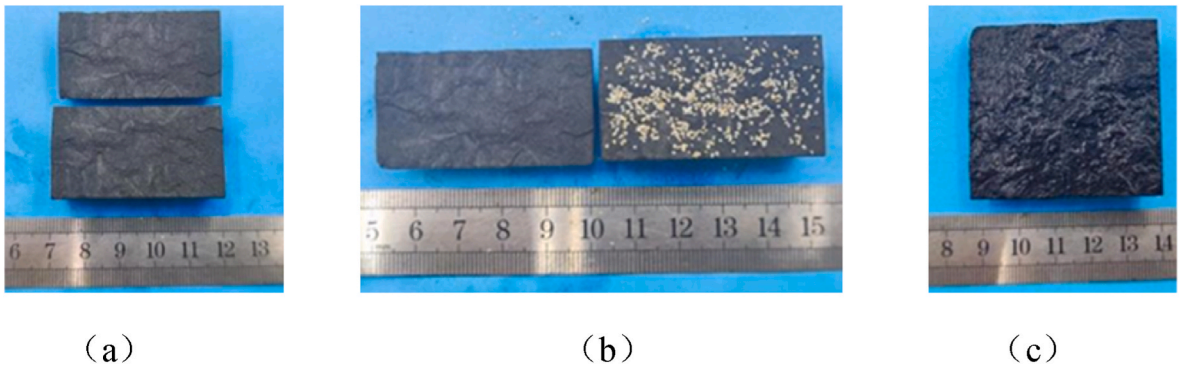

Fig. 17. Single layer laying of quartz sand (a) the rock fracture surface; (b) Quartz sand is laid on the fracture surface; (c) the rock fracture surface after stress-sensitive experiment.

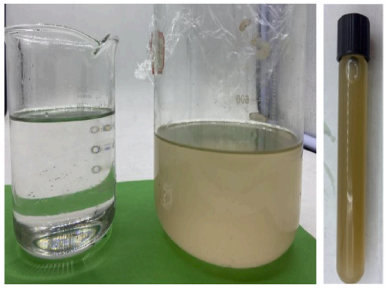

Fig. 18. Laying quartz sand: fluid before and after the experiment.

was not weakened, and group C rock sample was exposed to white oil containing 1% nanomaterials (Table 2).

(2) **Test of friction coefficient of fracture surface**

(1) Twenty-two spare rock samples were taken, and the evenly divided D1~D7, E1~E7, and F1~F7 rock samples were weighed and recorded. The remaining rock sample G was not soaked. The plugging material into the oven, 60 °C drying 24 h standby.

(2) Take three clean large capacity beakers, and put D, E and F cores into three beakers respectively, with the end face to be measured facing upwards. The same volume of white oil, NaOH solution (pH = 10) and oil-based drilling fluid filtrate were added to beakers of groups D, E and F respectively. The experimental fluid should completely immerse the rock sample. The soaking times of rock samples are 1day, 3days, 5days, 7days, 9days, 11days and 13days, respectively.

(3) Put the weight of 50g into the precision balance with the sensitivity of 0.1 mg for weighing, then open the friction coefficient measuring device, adjust the voltage control knob to set the voltage to 20V and reset the traction bracket, hang the weighed weight on the spring end of the traction bracket, and read out the tension value recorded by the tension sensor at this time. The measured tension value was divided by the gravity acceleration ($9.8m/S^2$) and compared with the weight value recorded by the balance. If the error margin was less than 1%, it indicated that the friction coefficient sensor was accurate, and the experiment could be continued. Otherwise, the tension sensor should be corrected in advance until the error was less than 1%.

(4) According to the proportion of 3% calcium carbonate + 5% NT-DS +0.5%GT-MF+0.2%LCC-200 fully mixed plugging materials, the mixed material was adhered to the friction plate in a

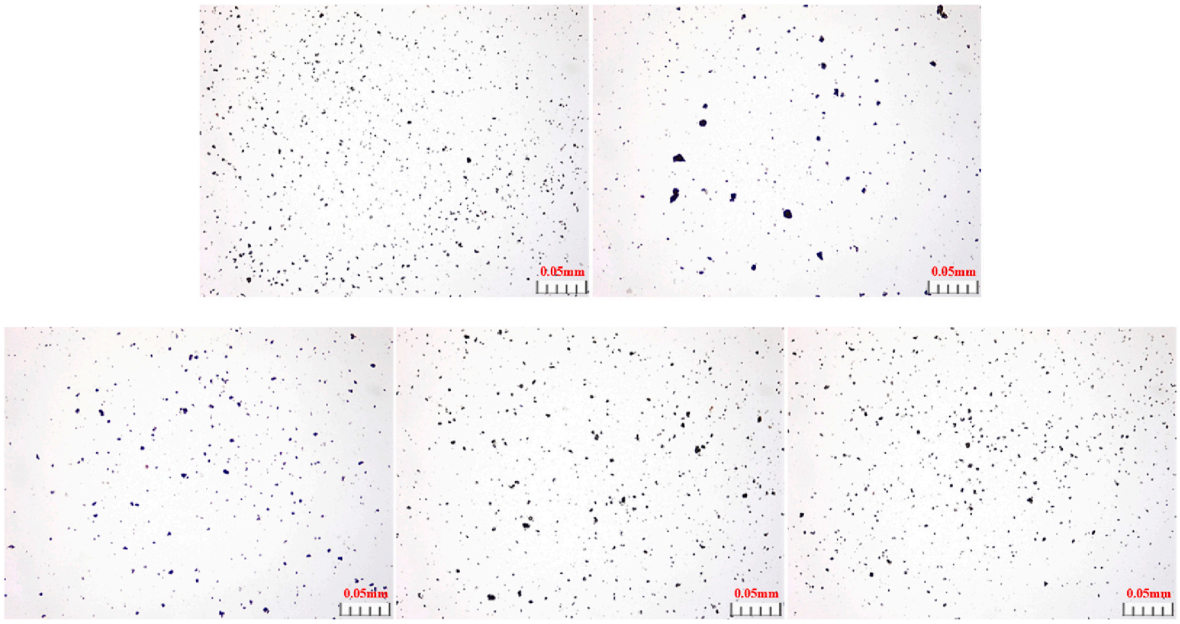

Fig. 19. Laying quartz sand: shale rock powder filtered from the outlet fluid.

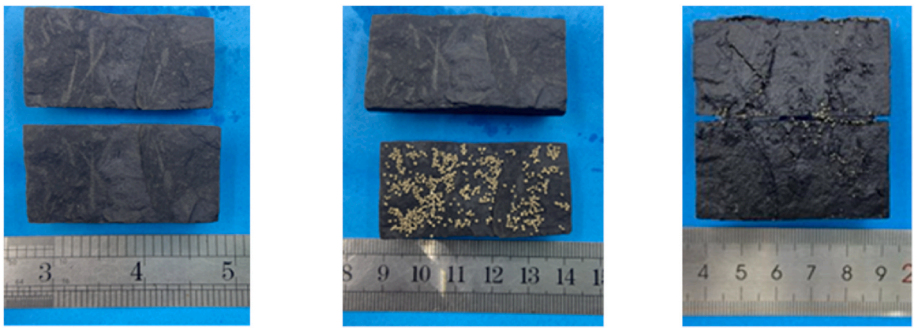

Fig. 20. Single layer paving of ceramsite (a) the rock fracture surface; (b) the ceramide is laid on the fracture surface; (c) the rock fracture surface after stress-sensitive experiment.

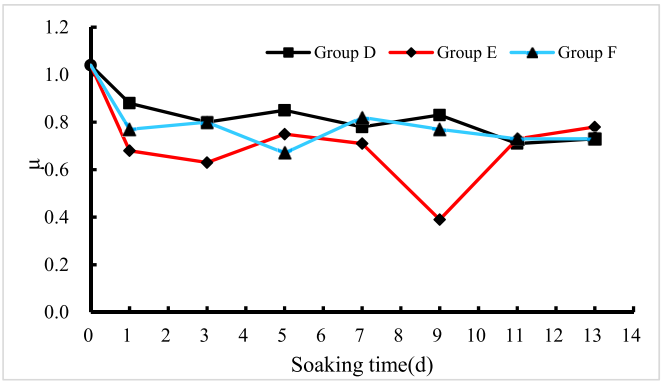

Fig. 21. Friction coefficient changes with liquid immersion time.

Table 6
Friction coefficient average of three experiment groups.

Group	Friction coefficient average	
	First	Second
D	0.80	0.78
E	0.67	0.64
F	0.76	0.73

single layer. Then the plugging materials were fixed by pressing the friction plate several times by hand.

(5) Take out the rock sample D1 soaked for 1day and use oil-absorbing paper to absorb the residual experimental fluid on the rock sample.
(6) Stick the friction plate of plugging material to the bracket, spray the white oil to the friction plate with the sprayer, D1 is connected to the traction spring to prevent the friction plate at the left end.
(7) Adjust the voltage control knob to set the voltage to 12V, click the software data recording button, open the motor start switch to start the friction coefficient measurement experiment.
(8) When the rock sample moves to the right end of the friction plate, stop the experiment and save the data. The traction bracket was reset to the initial position, the friction plate was remade, and the same experiment was repeated.
(9) Process the data and calculate the friction coefficient by Eq (2-1).
(10) Repeat steps (4)–(9) for the remaining 21 rock samples (Table 3).

3. Experimental results

3.1. Micron indentation test results

The test results of micron indentation are shown in Table 4. The elastic modulus of Group A samples ranges from 19.05 GPa to 31.39 GPa, and the compressive hardness ranges from 0.39 GPa to 0.99 GPa, with average values of 24.30 GPa and 0.64 GPa respectively. The elastic modulus of Group B samples is 13.19 GPã27.03 GPa, and the compressive hardness is 0.22 GPã0.63 GPa, with average values of 22.42 GPa and 0.63 GPa, respectively. The elastic modulus of rock samples in Group C ranges from 18.25 GPa to 30.76 GPa, and the compressive hardness ranges from 0.46 GPa to 0.88 GPa, with average values of 23.92 GPa and 0.62 GPa, respectively. The micron indentation test results of the three groups of rock samples show that white oil has no obvious weakening effect on the surface micromechanical properties of shale in a short time. The micromechanical properties of shale surface show strong heterogeneity. As shown in Figs. 7–9, the shale surface mechanical properties exhibit significant heterogeneity. The elastic modulus and indwelling hardness exhibit a similar variation trend and display a strong positive correlation. The experimental results indicate a decrease in the mechanical strength of the shale surface upon contact with white oil.

During the loading and stabilization process, the metal indenter reaches the maximum penetration depth of h_{max}. As the unloading phase concludes, the penetration depth of the indenter is recorded as hf, indicating plastic deformation of the shale surface (Fig. 10). In this paper, the ratio of h_f to h_{max} is utilized to represent the depth of compressive loss rate. As shown in Figs. 11–13, plastic failure is commonly observed on the shale surface under external loads. Furthermore, the depth of the compressive loss rate exhibits significant heterogeneity.

3.2. Friction coefficient test results

In the process of dragging, the rock sample is in a state of intermittent sliding. In this process, when the tension of the rock sample is greater than the maximum static friction force, it will slide, and the tension will quickly decrease to a certain value. When the rock sample stops sliding, the tension will increase rapidly, and the rock sample will start to slide again when the tension is greater than the maximum static friction force, and so on. In order to reduce experimental errors and avoid wasting data points, all the maximum values in the image were taken as the maximum static friction force on the rock sample, and the friction coefficient on the surface of the rock sample was calculated. The calculation results of the friction coefficient are shown in Table 5. After soaking, the friction coefficient on the surface of the three groups of rock samples decreased to different degrees, and showed a general trend of decreasing.

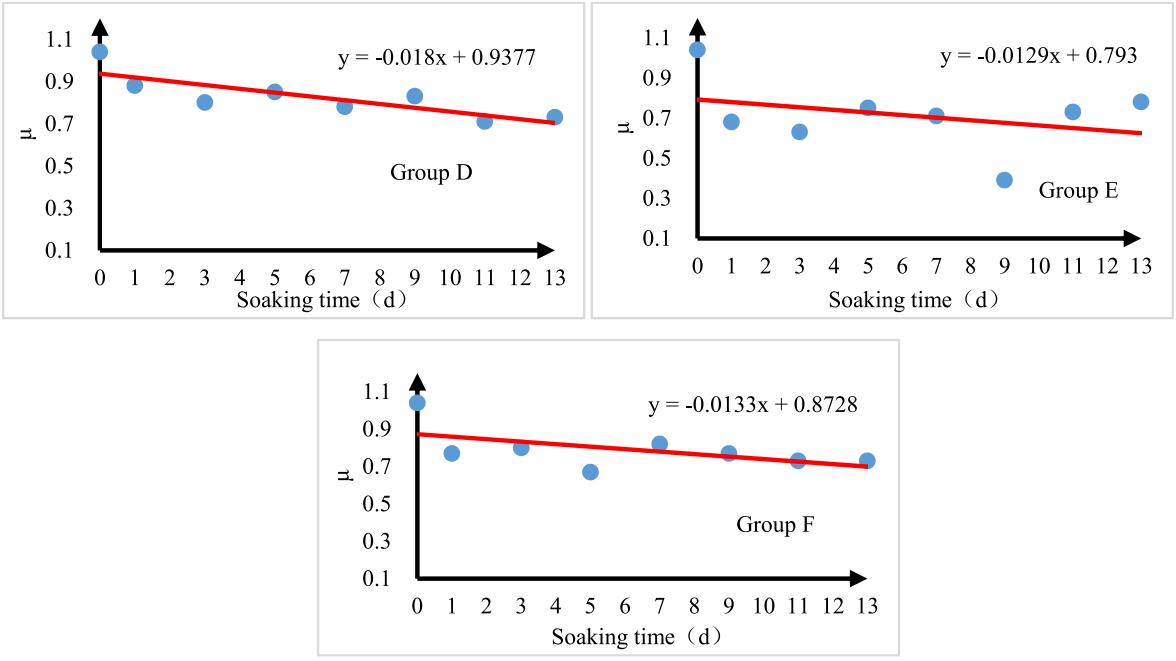

Fig. 22. Friction coefficient trend of the first test.

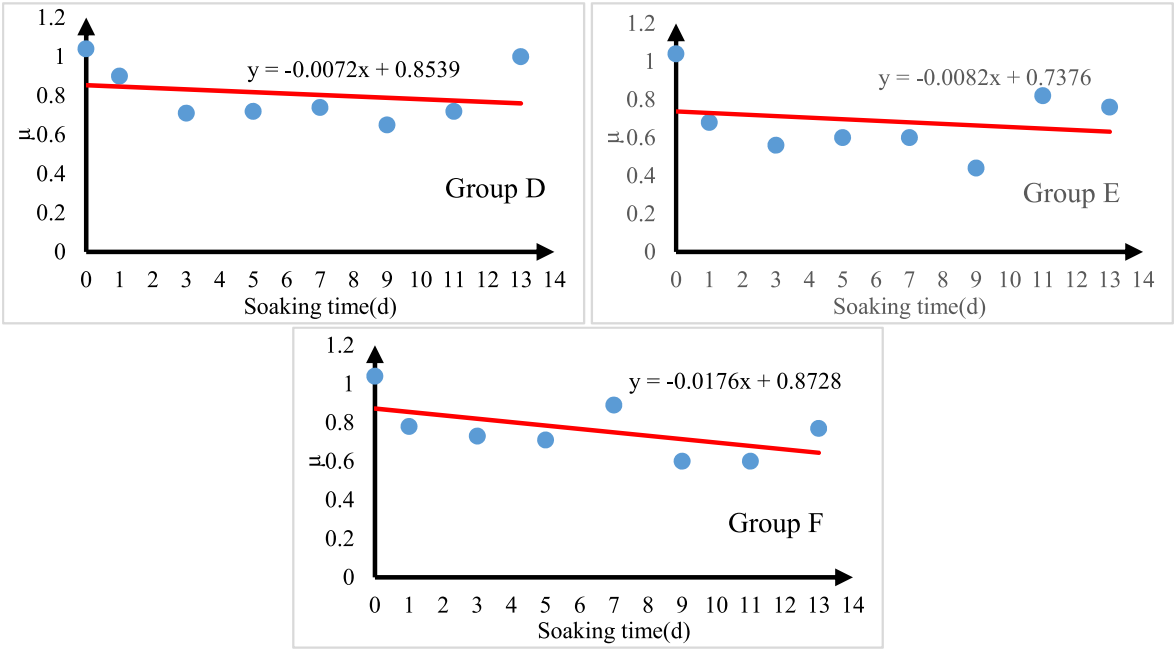

Fig. 23. Friction coefficient trend of the second test.

4. Results analysis

4.1. Influence of mechanical properties of fracture surface on plugging

Shale formations contain numerous micro-fractures that serve as channels for fluid intrusion. The extent of fluid intrusion into shale directly impacts the mechanical properties of its surface. To mitigate fluid intrusion, nanoparticles can be employed to effectively plug pores and micro-fractures. By selectively blocking these pathways, nanoparticles hinder fluid intrusion, as illustrated in Figs. 14 and 15. In Fig. 15c, the bright area depicted in the CT image indicates regions where fluid intrusion occurs, while the gray area represents zones where fluid is unable to infiltrate.

After averaging the penetration loss rate, the result indicates that group A < Group C < Group B (Fig. 16). Through comparison, the extent of damage to the shale surface can be determined. Upon contact with white oil, the resistance of the shale surface to damage decreases. It is observed that the value for Group C is slightly smaller than that of Group B, which could be attributed to the shorter fluid contact time and smaller maximum load in Group C.

A large number of studies have reported that working fluid immersion can reduce the mechanical properties of shale rock mass, which is manifested in the reduction of elastic modulus and brittleness on a macro scale. The mechanical properties of shale are affected by surface

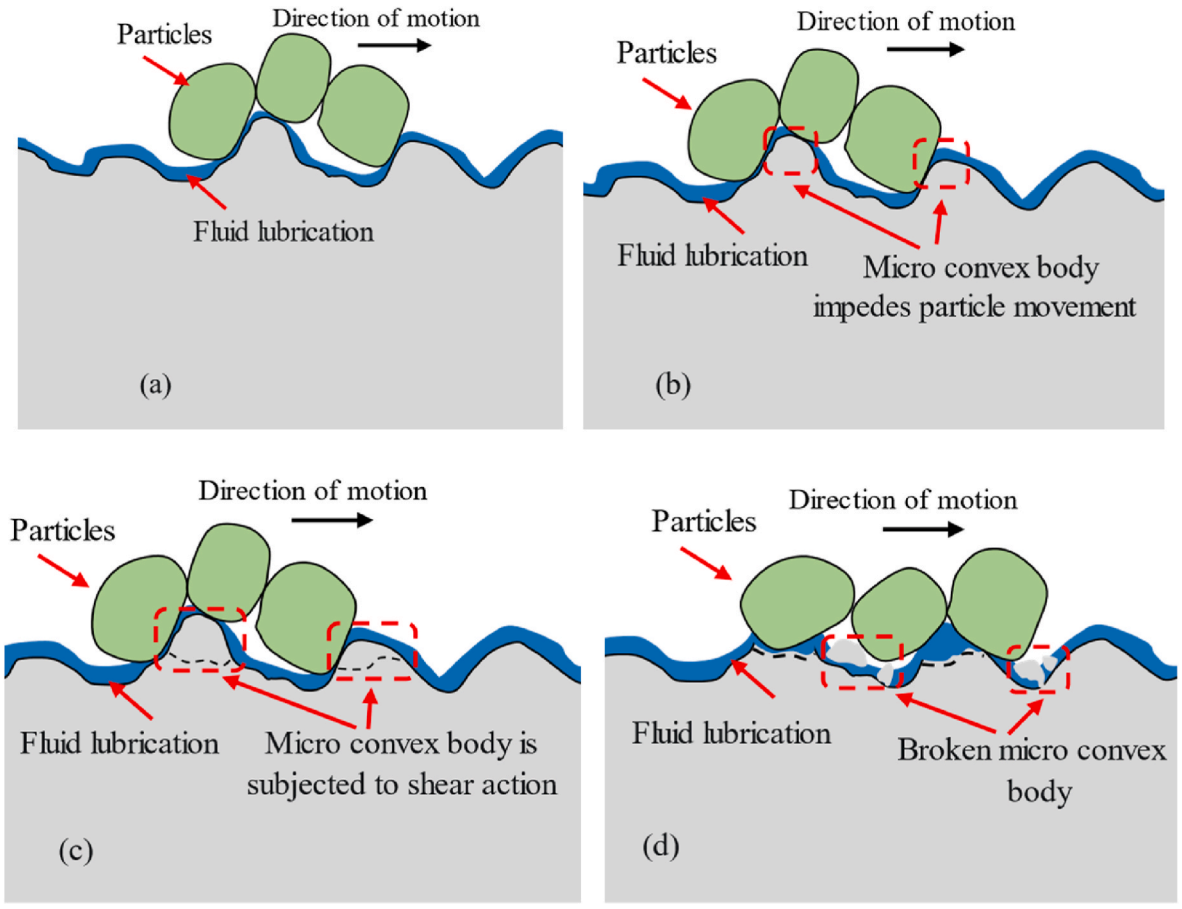

Fig. 24. Oil-based drilling fluid reduces the pressure bearing capacity of plugging zone.

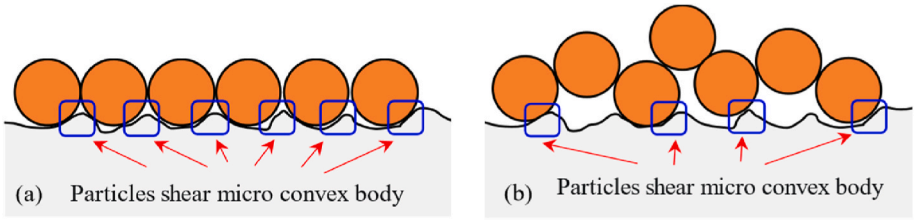

Fig. 25. The effective contact area between plugging materials and shale surface.

forces (such as van der Waals forces, solid-solid bonding or cementation) in contact with the particles, and direct intergranular outflow may be altered or destroyed by shale-fluid interactions (Spencer, 1981; Tutuncu and Sharma, 1992; Lu et al., 2020). The decrease of mechanical properties at the microscopic level of shale gradually accumulates, and finally affects the macroscopic mechanical properties of shale. The change of the surface mechanical properties of shale fractures affects the sealing effect, which is manifested by the pressure level of the plugging zone.

Britt and Schoeffler (2009) reported in their report that, according to U.S. shale data, when the static Young's modulus of shale is less than 24 GPa, the rock tends to be more ductile and unable to fracture (Britt and Schoeffler). When the mechanical strength of shale surface decreases, i.e, changing from brittle to plastic, the shale surface deformation may be intensified, and local breakage may occur. Under the effect of fracture closure stress, the granular materials in the plugging layer are more easily embedded into the rock mass, which enhances the pressure of the plugging layer and reduces the drilling fluid loss.

Figs. 17 and 20 show the fracture plugging experiment with rigid particles. After laying rigid particles on the fracture surface, a core gripper is placed and the damage is displaced with white oil for 24 h. (a) ~ (c) is the fracture surface of quartz sand monolayer, and (d) ~ (f) is the fracture surface of ceramic monolayer, where the compressive strength of ceramic is greater than that of quartz sand. 24 h later, the rock samples were taken out to observe the fracture surface. In the process of pressurized displacement, the quartz sand (c) was broken. Rock powder or unapparent fractures occurred on the fracture surface. The rock powder and broken quartz sand were driven out with the white oil (Figs. 18 and 19). The laid ceramides (f) did not break. Despite the presence of rock powder and noticeable fractures on the fracture surface, there was minimal or negligible white oil flow observed from the outlet.

During the plugging process, the oil-based drilling fluid that is difficult to filter into the formation from the fracture will continue to weaken the mechanical properties of the shale surface, which may break and affect the stability of the plugging zone structure. Due to the effects of ground stress, particles with lower strength are subjected to breakage. Variations in wellbore pressure can then induce these broken particles to etch the fracture surface, resulting in further fracture damage and

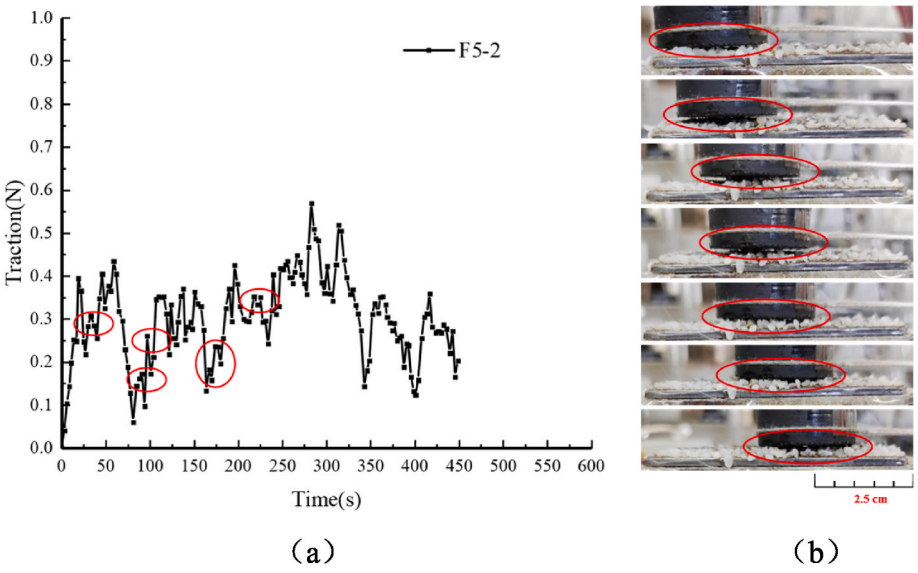

Fig. 26. The second test process of friction coefficient of F5 rock sample.

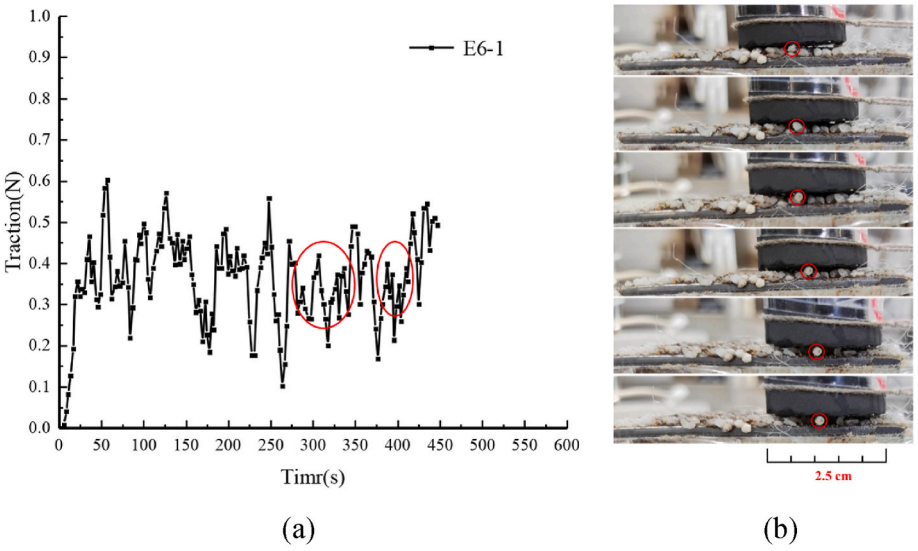

Fig. 27. The first test process of friction coefficient of E6 rock sample.

subsequently affecting the pressure within the plugging zone. Therefore, considering the weakening of the mechanical properties of shale surface and the trend of plastic transformation, materials with high compression resistance, high hardness and low sphericity should be considered in the selection of plugging materials. In addition, nanomaterials can be added to the plugging slurry to protect the fracture surface.

4.2. Effect of frictional quality of fracture surface on plugging

4.2.1. Effect of oil-based drilling fluid on friction coefficient of fracture surface

Fig. 21 shows the variation of friction coefficient and soaking time of rock samples. It can be seen from the figure that the friction coefficient of the three groups of rock samples all decreased to different degrees. The average friction coefficient across the three experimental groups is ranked as follows: Group D > Group F > Group E (Table 6). The results indicate that the lye demonstrates the most significant impact on reducing the friction coefficient of a rock surface, while the oil drilling fluid filtrate exhibits a slightly weaker effect. Lastly, the white oil displays the least weakening influence on the friction coefficient. The trend in the variation of the friction coefficient can be effectively analyzed by applying linear fitting to the data points representing the friction coefficient. Figs. 22 and 23 show that with the increase of soaking time, the friction coefficient of shale surface may further decrease, which has significant influence on the pressure of the plugging layer.

A large number of studies have shown that clay minerals, quartz and feldspar in shale can react with alkali (Yu et al., 2013; Yu, 2013; Soler, 2003; Kang et al., 2014b). Clay minerals, quartz and other minerals in sandstone will be eroded by lye, which leads to erosion holes in sandstone strata, greatly reducing mechanical properties and instability (Southwick, 1985; Mohnot et al., 1987; Chen et al., 1996; Feng et al., 2010). Shale generally contains a large number of clay minerals, quartz and other substances. The erosion effect of lye on shale leads to the increase of erosion pores, the rock structure becomes loose, and the mechanical strength decreases (Yu et al., 2013). You et al. discussed the influence of lye erosion on borehole stability. They maintained the weak alkalinity of drilling fluid (pH 8.0–8.5) in the shale drilling site of

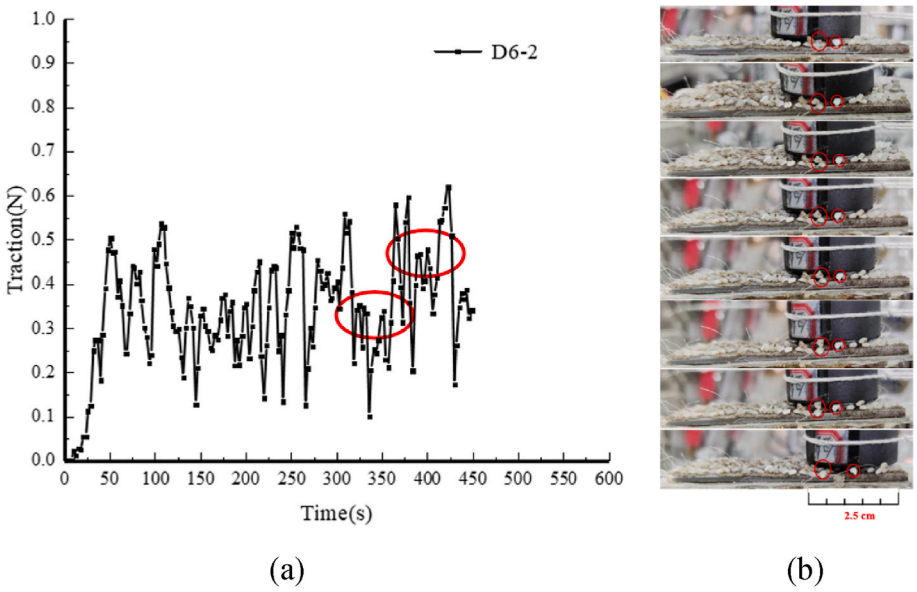

Fig. 28. The second test process of friction coefficient of D6 rock sample.

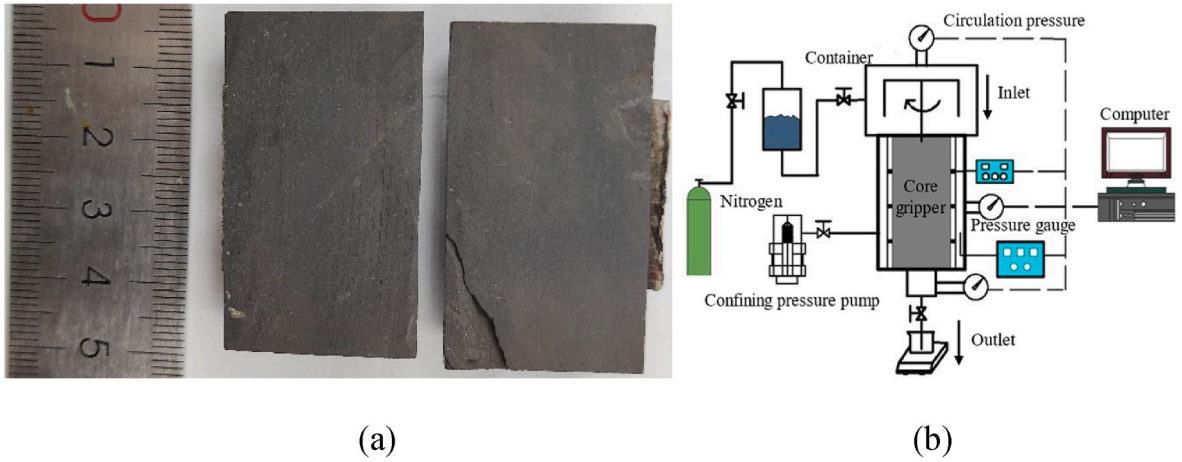

Fig. 29. (a) Fracture sample; (b) Schematic diagram of leak containment experiment equipment.

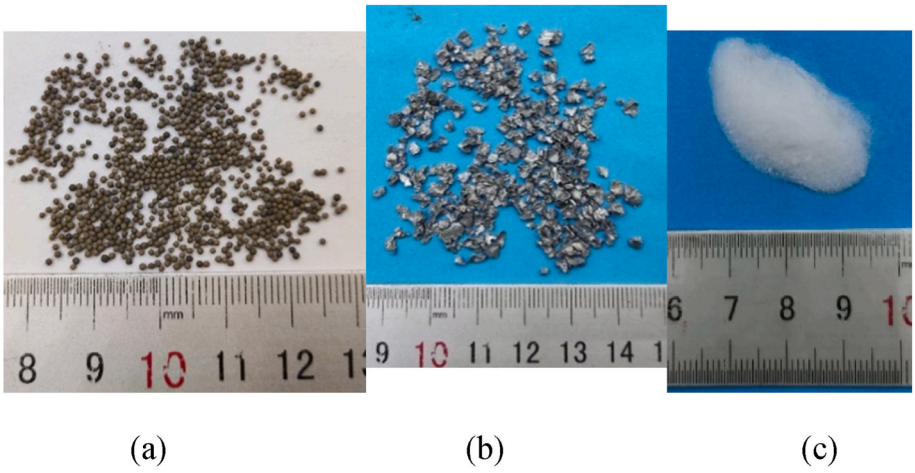

Fig. 30. Experimental material.

Table 7
Experimental material properties.

Material property	GYD	$CaCO_3$	ceramsite
friction coefficient	1.23	0.95	–
Compressive strength/D90 crushing rate MPa/%	–	25/22.7%	45/4.2%
sphericity	0.53	0.88	–

Table 8
Experimental fluids.

Formulation number	Fluid displacement	Formulation	Fracture parameter
1	–	OBF+3%$CaCO_3$+0.2% LCC-200+ 5%NT-DS+0.5%GT-MF	Inlet width1.5 mm Outlet width 1 mm
2	OBF	OBF+3%$CaCO_3$+0.2% LCC-200+ 5%NT-DS+0.5%GT-MF	
3	OBF+1% nanomaterial	OBF+3%$CaCO_3$+0.2% LCC-200+ 5%NT-DS+0.5%GT-MF	
4	OBF	OBF+3%GYD+0.2% LCC-200+ 5%NT-DS+0.5%GT-MF	
5	OBF	OBF+3% Ceramsite+0.2%LCC-200+ 5%NT-DS+0.5%GT-MF	

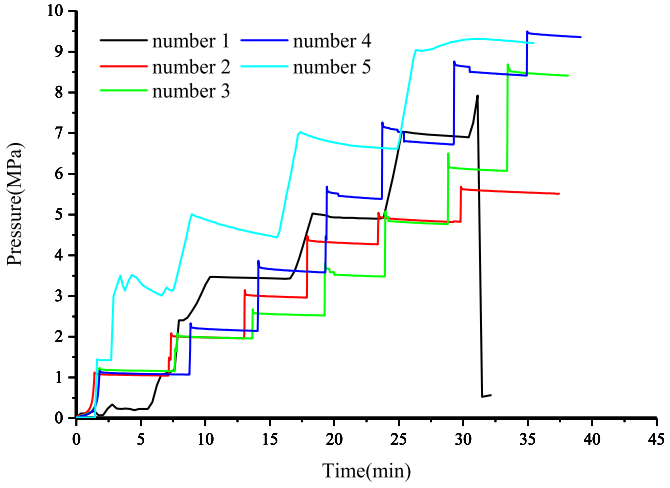

Fig. 31. Plugging pressure history of shale fractures.

Huimin Sag of Shengli Oilfield, eliminated the influence of hydration and weakened the lye erosion, and significantly improved the borehole stability (You et al., 2013). She Jiping also pointed out that after the reaction of lye with shale surface minerals, the shale surface becomes smoother, mineral particles fall off, and a large number of dissolution pores are generated, reducing the mechanical properties (She, 2016).

Based on the analysis conducted, two primary mechanisms can be identified through which oil-based drilling fluid reduces the friction coefficient of shale surfaces. One is the lubrication of oil-based drilling fluid. The other is the alkali erosion. In Fig. 24, the oil-based drilling fluid forms a liquid film on shale surface. This layer of liquid film plays a lubricating role and reduces the friction coefficient between particles and fracture surface. In Fig. 24b, c and 24d, the movement of particles is impeded by the presence of micro-convex bodies, thereby hindering their mobility. The immersion of oil-based drilling fluid leads to a reduction in the shear strength of micro-convex bodies, consequently decreasing the pressure-bearing capacity of the plugging zone.

4.2.2. *Friction behavior analysis*

The previous section has examined the impact of oil-based drilling fluid on the friction coefficient of fracture surface. In this section, we will discuss the influence of contact modes between particles and the shale surface on the bearing pressure of the plugging zone. Due to the influence of fluid environment and the morphologic parameters of plugging materials, the contact modes between materials in plugging layer and fracture surface are complex and diverse, and the different contact modes will directly affect the friction coefficient (Xu et al., 2022, 2023). In this paper, the influence of the contact mode between plugging material and fracture surface on the friction coefficient is analyzed.

When there is a large effective contact area between the plugging materials and the shale surface, a higher number of shear micro-convex bodies are observed (Fig. 25a). Conversely, when the effective contact area is small, the number of shear micro-convex bodies in the plugging materials decreases (Fig. 25b). The presence of a greater number of shear micro-convex bodies results in increased resistance between the shale surface and the materials, leading to a macroscopic increase in friction. In the second friction coefficient test process of rock sample F5 as shown in Fig. 26, (b) recorded the changes of effective contact area between plugging material and rock sample surface during the test. In (b), the effective contact area between the plugging material and the rock sample surface decreases for several times. In (a), the maximum value of the corresponding tension decreases for several times.

When particles are no longer at rest, the friction between particles rolling on the fracture surface also decreases. In the process of friction coefficient test as shown in Figs. 27 and 28, the rolling of particles reduces the tension value, indicating that the friction between the crack surface and the plugging material is small during this period. In addition, the rolling behavior of the particle material also reduces the friction between the two, and the particle movement may break the balance of other materials, thus affecting the bearing capacity of the plugging zone.

4.3. *Leak containment experiment*

To validate the impact of the mechanical properties of shale fracture surfaces on the strength of the plugging zone, a series of leakage containment experiments were conducted. Fig. 29 shows the schematic diagram of the rock sample and experimental instrument. The fracture surface of the sample was pressurized in contact with the oil-based drilling fluid for 24 h, then the leakage prevention experiment was conducted. High-strength particles (Fig. 30a), high-friction materials

Table 9
Experimental fluid leakage details.

Number	Pressure/Cumulative loss (MPa/mL)								
	1	2	3	4	5	6	7	8	9
1	0.2	0.2	0.2	0.2	0.3	0.3	leakage		
2	0.15	0.2	0.5	1.3	leakage				
3	0.1	0.1	0.5	0.9	1.1	1.8	2.0	leakage	
4	0.08	0.2	0.65	0.7	0.9	1.4	1.7	2.3	leakage
5	0.12	0.25	0.6	1.5	1.9	2.0	2.4	2.8	leakage

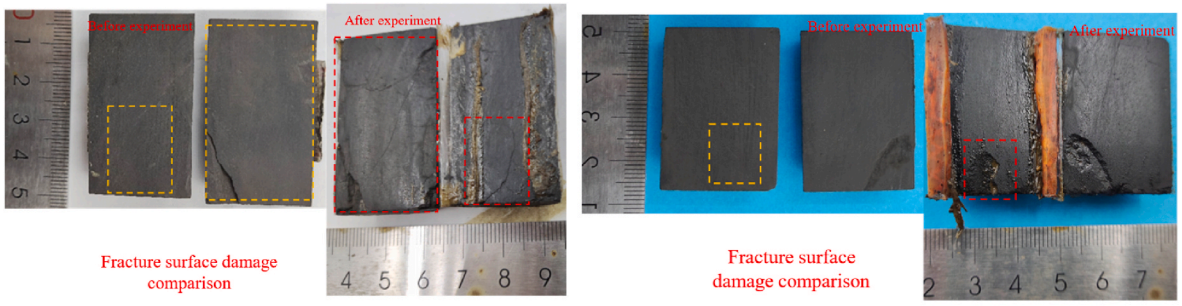

(a) (b)

Fig. 32. Fracture surface damage comparison (a) Formulation number 2; (b) Formulation number 3.

(Fig. 30b) and nanomaterials (Fig. 30c) were selected for the experiment. Table 7 displays the material properties obtained from the experimental measurements. Table 8 lists the contact fluid and plugging slurry formulations of the sample.

Fig. 31 illustrates the results obtained from the experiment, indicating that the maximum pressure achieved varied in the following order: number 4 > number 5 > number 3 > number 1 > number 2. It is worth noting that throughout the experiment, there was minimal or negligible loss of plugging slurry, as indicated in Table 9. Based on the analysis of the experimental results, the following insights can be derived:

(1) Comparison between formulations 1 and 2: Immersing the fracture in oil-based drilling fluid leads to a decrease in the pressure-bearing capacity of the plugging zone.
(2) Comparison between formulations 2 and 3: After the experiment, significant cracks and fractures were observed on the fracture surface (Fig. 32a). The presence of nanomaterials acts as a protective measure, resulting in fewer visible cracks and fractures on the fracture surface.
(3) Comparison between formulations 2 and 4: The plugging zone formed using high friction materials exhibits a higher pressure-bearing capacity.
(4) Comparison between formulations 2 and 5: In the experiment, calcium carbonate particles experience breakage, whereas ceramsites remain intact, resulting in a larger bearing capacity for formulation 5. However, the friction coefficient of ceramsite is smaller than that of calcium carbonate, making the plugging zone more prone to movement. This could be a contributing factor to the decrease observed in the pressure curve.

5. Conclusion

Through extensive research, this paper has derived the following key conclusions:

(1) Prolonged exposure of shale to oil-based drilling fluid leads to a reduction in its surface mechanical strength. Consequently, the shale surface becomes more susceptible to fragmentation, compromising the stability of the plugging zone.
(2) The contact of shale with oil-based drilling fluid results in a decrease in the friction coefficient of the shale surface. This decrease in friction coefficient diminishes the pressure bearing capacity of the plugging zone.
(3) To enhance the pressure bearing capacity of the plugging zone, the selection of high-strength materials, high-friction coefficient materials, and nanomaterials is recommended. These materials can effectively reinforce the plugging zone and mitigate the adverse effects caused by fluid interaction.

By identifying these conclusions, this research provides valuable insights into the control of losses and the stabilization of wellbore walls in shale drilling. These findings serve as a foundation for further advancements in the optimization of drilling practices in shale gas reservoirs.

Having established the direct influence of shale fracture surface mechanical properties on the bearing capacity of the plugging zone, several promising future research directions can be suggested. Specifically, the focus will be shifted towards investigating the compatibility between the mechanical properties of shale fracture surfaces and various plugging materials. Next, develop systematic selection methods for plugging materials based on the specific mechanical properties of shale fracture surfaces. By considering the unique characteristics of the shale formation, these methods can aid in the precise selection of plugging materials to optimize the integrity and stability of the plugging zone. Furthermore, conduct comprehensive experimental studies to validate the findings and conclusions of this research on a larger scale. Field-scale experiments and simulations can provide valuable insights into the practical application and effectiveness of the observed effects.

Credit author statement

Chengyuan Xu: Methodology, Formal analysis, Investigation, Writing – original draft. Lingmao Zhu: Formal analysis, Investigation, Writing – original draft. Feng Xu: Formal analysis, Validation, Writing - review & editing. Yili Kang: Methodology, Investigation, Resources. Haoran Jing: Formal analysis, Investigation. Zhenjiang You: Formal analysis, Writing - review & editing, Review.

Declaration of competing interest

The authors declare that they have no known competing financial interests or personal relationships that could have appeared to influence the work reported in this paper.

Data availability

Data will be made available on request.

Acknowledgements

The authors gratefully acknowledge the financial support from the National Natural Science Foundation of China (Grant Nos. 52274009 and 51604236), the Sichuan Province Youth Science and technology innovation team project (Grant No. 2021JDTD0017), and the Sichuan Province Science and Technology Project (Grant No. 2018JY0436).

Acronyms

CFD Computational fluid dynamics

DEM	Discrete element method
LCM	Lost circulation material
SIF	Stress intensity factor

Nomenclature

μ_f	The friction coefficient, dimensionless
F_f	The tension value recorded by the sensor, N
W_N	The mass of friction slider, kg
E	The surface elastic modulus of shale, GPa
H	The surface hardness of the shale, GPa
$h_{\max}$	The maximum penetration depth of the indenter during the steady load phase, mm
h_f	The minimum penetration depth of the indenter during the unloading phase, mm

References

Alstadt, K.N., Katti, K.S., Katti, D.R., 2015. Nanoscale morphology of kerogen and in situ nanomechanical properties of Green River Oil Shale. J. Nanomech. Micromech. 6 (1), 04015003.

Bennett, K.C., Berla, L.A., Nix, W.D., et al., 2015. Instrumented nanoindentation and 3D mechanistic modeling of a shale at multiple scale. Acta Geotechnica 10 (1), 1–14.

Britt, L.K., Schoeffler, J. The geomechanics of a shale play: what makes a shale prospective. In: SPE Eastern Regional Meeting. Society of Petroleum Engineers..

Chen, Zhong, Luo, Zhetan, Shen, Mingdao, et al., 1996. From the chemical behavior of reservoir minerals in alkaline displacing agents to the formation of raw pores in sandstone reservoirs. J. SW Petrol. Univ. (2), 17–21.

Chen, Ping, Han, Qiang, Ma, Tianshou, et al., 2015. The mechanical properties of shale based on micro-indentation test. Petrol. Explor. Dev. 42 (5), 662–670.

Deirieh, A., Ortega, J.A., Ulm, F.J., et al., 2012. Nanochemomechanical assessment of shale : A coupled WDS-indentation analysis. Acta Geotechnica 7 (4), 271–295.

Feng, Xiating, Ding, Wuxiu, Yao, Huayan, et al., 2010. Coupled Chemical Stress Effect on Rock Fracturing Process [M]. Science Press, Beijing, pp. 16–266.

Jia, Suogang, Wang, Youyu, Wang, Qian, et al., 2021. Research on the micro-scale method for testing the mechanical anisotropy of shale. J. Geomechanics 27 (1), 10–18.

Kang, Yili, Xu, Chengyuan, Tang, Long, et al., 2014a. Constructing a tough shield around the wellbore: theory and method for lost-circulation control. Petrol. Explor. Dev. 41 (4), 473–479.

Kang, Yili, Huang, Fansheng, You, Lijun, et al., 2014b. Simulation and application of shale fracture width immersed in drilling fluid. Oil Drill. Prod. Technol. 36 (5), 41–46.

Kang, Yili, Wang, Kaicheng, Xu, Chengyuan, et al., 2019. High-temperature aging property evaluation of lost circulation materials in deep and ultra-deep well drilling. Acta Pet. Sin. 40 (2), 215–223.

Kumar, V., Sondergeld, C.H., Rai, C.S., 2012. Nano to Macro Mechanical Characterization of Shale [C]//SPE Annual Technical Conference and Exhibition. SPE, San Antonin, 159804.

Lavrov, 2016. Lost Circulation: Mechanisms and Solutions. Gulf professional publishing.

Liu, Shengxin, Wang, Zongxiu, Zhang, Linyan, et al., 2018a. Micromechanics properties analysis of shale based on nano-indentation. J. Exp. Mech. 33 (6), 957–968.

Liu, Xiugang, Hao, Shijun, Liu, Xiutai, et al., 2018b. Mechanical characteristics of downhole and outcrop Longmaxi shale in weiyuan block, sichuan province. West-China Explor. Eng. 30 (3), 98–101.

Lu, Yunhu, Li, Yucheng, Wu, Yongkang, et al., 2020. Characterization of shale softening by large volume-based nanoindentation. Rock Mech. Rock Eng. 53 (3), 1393–1409.

Mohammadizadeh, S.M., Azhdary, M.M., Talebbeydokhti, N., 2021. Analysis of flow in porous media using combined pressurized-free surface network. Porous Media 24 (10), 1–15.

Mohnot, S.M., Bae, J.H., Foley, W.L., 1987. A study of mineral/alkali reactions [R]. SPR 13032.

Ni, X.X., Jiang, G.C., Wang, J.H., et al., 2021. Study on a lyophobic nanophase plugging agent for oil base muds. Drill. Fluid Complet. Fluid 38 (3), 298–304.

Rehm, B., Schubert, J., Haghshenas, A., Paknejad, A.S., 2008. Managed Pressure Drilling. Gulf Publishing Company, Houston (TX).

She, Jiping, 2016. Catastrophic Instability Mechanism to System Consisted of Plugging Zone and Rock in Shale Formation [D]. Southwest Petroleum University.

She, Jiping, Zhang, Hao, Han, Kai, et al., 2020. Experimental investigation of mechanisms influencing friction coefficient between lost circulation materials and shale rocks. Powder Technol. 364, 13–26.

Shi, Xian, Jiang, Xu, Lu, Shuangfang, et al., 2019. Investigation of mechanical properties of bedded shale by nanoindentation tests: a case study on Lower Silurian Longmaaxi Formation of Youyang area in southeast Chongqing, China. Petrol. Explor. Dev. 46 (1), 155–164.

Soler, J.M., 2003. Reactive transport modeling of the interaction between a high-pH plume and a fractured marl: the case of Wellenberg. Appl. Geochem. 18 (10), 1555–1571.

Song, Li, Kang, Yili, Li, Daqi, et al., 2015. Numerical investigation into the influence of plug zone on fracture deformation in lost circulation controlling. Nat. Gas Geosci. 26 (10), 1963–1971.

Southwick, J.G., 1985. Solubility of silica in alkaline solutions implications for alkaline flooding. SPE J. 25 (6), 857–864.

Spencer Jr., J.W., 1981. Stress relaxations at low frequencies in fluid-satu-rated rocks: Attenuation and modulus dispersion. J. Geophys. Res: Solid Earth 86, 1803–1812.

Sun, Jingsheng, Xu, Chengyuan, Kang, Yili, et al., 2020. Research progress and development recommendations covering damage mechanisms and protection technologies for tight/shale oil and gas reservoirs. Petrol. Drill. Tech. 48 (4), 1–10.

Tutuncu, A.N, Sharma, M.M., 1992. The influence of fluids on grain contact stiffness and frame moduli in sedimentary rocks. Geophysics 57, 1571–1582.

Wang, W.J., 2020. Development and application of nano plugging agent with core-shell structure for shale strata. Sci. Technol. Eng. 20 (9), 3585–3590.

Wang, H., Soliman, M., Towler, B., 2008. Investigation of factors for strengthening a wellbore by propping fractures. In: Proceedings of SPE/IADC Drilling Conference. Florida. SPE 112629; 4–6 March.

Wang, Gui, Pu, Xiaolin, Wen, Zhiming, et al., 2011. Mechanism of controlling lost circulation in induced fracture based on fracture mechanics. J. SW Petrol. Univ. 33 (1), 131–134+19.

Wang, Daobing, Zhou, Fujian, Hongkui, Ge, 2015. Et al. An experimental study on the mechanism of degradable fiber-assisted diverting fracturing and its influencing factors. J. Nat. Gas Sci. Eng. 27, 260–273.

Xu, Chengyuan, 2015. Models and Methods to Strengthen Wellbore Pressure Containment by Fracture Plugging in Fractured Reservoirs [D]. Southwest Petroleum University.

Xu, Chengyuan, Yan, Xiaopeng, Kang, Yili, et al., 2019. Friction coefficient: a significant parameter for lost circulation control and material selection in naturally fractured reservoir. Energy 174, 1012–1025.

Xu, Chengyuan, Yan, Xiaopeng, Kang, Yili, et al., 2020. Structural failure mechanism and strengthening method of plugging zone in deep naturally fractured reservoirs. Petrol. Explor. Dev. 47 (2), 399–408.

Xu, Chengyuan, Zhang, Jingyi, Kang, Yili, et al., 2021. Structural formation and evolution mechanisms of fracture plugging zone. Petrol. Explor. Dev. 48 (1), 202–210.

Xu, C.Y., Zhang, H.L., Kang, Y.L., et al., 2022. Physical plugging of lost circulation fractures at microscopic level. Fuel 317, 123477.

Xu, C.Y., Zhang, H.L., She, J.P., et al., 2023. Experimental study on fracture plugging effect of irregular-shaped lost circulation materials. Energy 276, 127544.

Yan, Xiaopeng, Xu, Chengyuan, Kang, Yili, et al., 2020a. Mesoscopic structure characterization of plugging zone for lost circulation control in fractured reservoirs based on photoelastic experiment. J. Nat. Gas Sci. Eng. 79, 10333.

Yan, Xiaopeng, Kang, Yili, Chengyuan, Xu, 2020b. Et al. Fracture plugging zone for lost circulation control in fractured reservoirs: multiscale structure and structure characterization methods. Powder Technol. 370, 159–175.

Yan, Xiaopeng, Xu, Chengyuan, Kang, Yili, et al., 2021. Mechanical mechanism of meso-structure instability plugging zone based on the characterization of force chain network. Acta Pet. Sin. 42 (6), 765–775.

You, Lijun, Kang, Yili, Li, Xiangchen, 2013. Mitigating borehole instability and formation damage with temporary shielding drilling fluids in low permeability fractured reservoirs [R]. SPE 165133.

Yu, Yangfeng, 2013. Multi-scale Structure Description and Borehole Instability Mechanism of Organic Rich Shale [D]. Southwest Petroleum University.

Yu, Yangfeng, Kang, Yili, You, Lijun, et al., 2013. Alkali corrosion: a new mechanism of shale borehole instability. Acta Pet. Sin. 34 (5), 983–988.

Zheng, Liu, Li, Maosen, et al., 2021. A technology for oil-swelling lost-circulation prevention and control while drilling and its application to shale gas wells, Sichuan-Chongqing area. Natural Gas Exploration and Development 44 (1), 118–124.

Zhu, W., Hughes, J.J., Bicanic, N., et al., 2007. Nanoindentation mapping of mechanical properties of cement paste and natural rocks. Materials Characterization 58 (11–12), 1189–1198.